ADVANCED SUSTAINABLE SYSTEMS
www.advsustainsys.com

Facile Self-Forming Superionic Conductors Based on Complex Borohydride Surface Oxidation

*Xiaoxuan Luo, Aditya Rawal, Claudio Cazorla, and Kondo-Francois Aguey-Zinsou**

Complex hydrides have attracted significant attention as better inorganic solid-state electrolytes owing to their lightweight and good compatibility with metal anodes (Li, Na, and/or Mg) for all solid-state batteries. However, high ionic conductivity is usually observed at high temperatures upon the stabilization of adequate crystalline phases enabling fast ionic mobility. Here, an extremely simple strategy to significantly increase the ionic conductivity of complex borohydrides is reported. By exposing complex borohydrides to oxygen, the rearrangement of surface atoms upon the oxidation of borohydride particles and the resulting defects lead to extremely high ionic conductivity. $NaBH_4$ and $LiBH_4$ exposed to 5% O_2 show an ionic conductivity of $\approx 10^{-3}$ S cm^{-1} at 35 °C. Similarly, oxidized $Mg(BH_4)_2$ displays a conductivity of $\approx 10^{-6}$ S cm^{-1} at 25 °C instead of 9.63×10^{-13} S cm^{-1}. To the best of the authors' knowledge, this is to date, the simplest approach to tune the properties of borohydrides toward high ionic conductivity at room temperature as it does not rely on the difficult synthesis of large cage boron based anions to substitute BH_4^- and allow better ionic conduction paths. Owing its simplicity, the finding has the potential to enable new avenues toward the realization of viable complex borohydride based solid-state electrolytes.

1. Introduction

Electrolytes are the heart of fully operational batteries. Their ability to ensure high ionic transport while enabling the electrodes to effectively function determines, to some extent, batteries' performances. Conventional metal-ion based batteries often rely on organic liquid electrolytes to operate.[1] These electrolytes have high ionic conductivity, but their flammability incurs safety issues,[2] while their reactivity at the electrode/electrolyte interface induces intrinsic deteriorations in battery performances while limiting the overall cell voltage and current density.[3]

In this respect, the prospect of all-solid-sate batteries has generated significant interest and considerable progress has been made toward the development of better solid-state-electrolytes.[4] In particular, many recent efforts have focused on alternative electrolytes for lithium (Li) based batteries but also all-solid state sodium (Na) batteries owing to their potential to provide a low cost alternative for the large scale storage of energy at the grid level.[4a,5]

To date, several solid Li conductors have been reported with conductivities in the range of 10^{-3} –10^{-2} S cm^{-1} at ambient temperature. This includes oxide based Li conductors such as lithium lanthanum titanates,[6] glass ceramics,[7] garnet types,[8] and sulfide based conductors.[9] However, once assembled into a full cell, the performance achieved with these electrolytes are inferior to conventional liquid electrolytes.[10] Current solid state Li conductors suffer from extensive reactivity with Li metal and/or high ohmic resistance, large interfacial resistance at the electrolyte/electrode interface and sometimes there are significant drawbacks in their fabrication method.

Progress along the development of solid-state electrolytes for Na batteries has been slower. Na electrolytes based on Na-β''-alumina and NASICON type conductors remain the best, exhibiting high ionic conductivities of 0.2–0.4 S cm^{-1} at 300 °C.[11] Hence, a major drawback in the use of Na-β''-alumina is the need of high operational temperatures, because the ionic conductivity is heavily compromised at low temperatures. The Sc modified NASICON, $Na_{3.4}Sc_{0.4}Zr1_{.6}(SiO_4)_2(PO_4)$, has been reported to exhibit a high ionic conductivity of 4×10^{-3} S cm^{-1} at 25 °C.[12] But NASICON type conductors have been shown to degrade when in contact with metallic Na.[13]

To date, a viable commercial option for all solid state batteries has been difficult to realize because of challenges in achieving: i) high ionic conductivities (>10^{-3} S cm^{-1}) at the ambient temperature while ensuring low electronic conductivity (<10^{-12} S cm^{-1}), ii) appropriate electrolyte/electrode contact, and iii) high stability of the electrode/electrolyte interface during battery operation.

Recently, through the study of the hydrogen storage properties of metal borohydrides, it has been found that lithium

X. Luo, Prof. K.-F. Aguey-Zinsou
MERLin
School of Chemical Engineering
The University of New South Wales
Sydney, NSW 2052, Australia
E-mail: f.aguey@unsw.edu.au
Dr. A. Rawal
NMR Facility
Mark Wainwright Analytical Centre
The University of New South Wales
Sydney, NSW 2052, Australia
Dr. C. Cazorla
School of Materials Science and Engineering and Integrated Materials Design Centre
The University of New South Wales
Sydney, NSW 2052, Australia
The ORCID identification number(s) for the author(s) of this article can be found under https://doi.org/10.1002/adsu.201900113.

DOI: 10.1002/adsu.201900113

borohydride ($LiBH_4$) displays an exceptionally high ionic conductivity of $\approx 10^{-3}$ S cm^{-1} when the material is heated above 120 °C to transition from its orthorhombic *Pmma* to the hexagonal $P6_3mc$ phase.[14] The advantage of $LiBH_4$ over other solid electrolytes is in its good chemical stability, its compatibly with Li electrodes over a wide electrochemical window and oxidative stability (>5V versus Li/Li$^+$).[14a,15] However, the high operating temperature $LiBH_4$ as a solid-state electrolyte hinders practical use.[16] Significant efforts have been made to alter the hexagonal phase and create an off-stoichiometric structure with high ionic conductivity at low temperatures.[17] This includes doping strategies with high polarizable anions larger than $[BH_4]^-$ to generate a high concentration of Frenkel defects. For example, through replacing $[BH_4]^-$ by the larger I^- anion an ionic conductivity of $\approx 10^{-5}$ S cm^{-1} at 60 °C has been reported.[18] Through the combination of $[BH_4]^-$ and $[NH_2]^-$ anions, a higher ionic conductivity of 2×10^{-4} S cm^{-1} at 25 °C for $Li_2(BH_4)(NH_2)$ was also reported.[19] This was explained by the possibility to generate through the $Li_2(BH_4)(NH_2)$ structure plural Li^+ occupation sites. Similar findings were also reported for $Na(BH_4)_{0.5}(NH_2)_{0.5}$, 2×10^{-6} S cm^{-1} at 27 °C,[20] and $Mg(BH_4)(NH_2)$, 3×10^{-6} S cm^{-1} at 100 °C.[21] By encapsulating $LiBH_4$ into a silicon dioxide scaffold (MCM-41) a higher ionic conductivity of $\approx 10^{-4}$ S cm^{-1} at 40 °C has also been claimed and this was attributed to fast $[BH_4]^-$ reorientation at the MCM-41 wall /$LiBH_4$ interface.[22] The effect of larger size anions including $[B_{12}H_{12}]^{2-}$, $[B_{10}H_{10}]^{2-}$, and $CB_9H_{10}^-$ was also investigated.[23] The highest conductivities, > 10^{-2} S cm^{-1}, were reported for Li and Na based $CB_9H_{10}^-$ at temperatures above 100 °C.[24] However, the synthesis of such compounds is rather complicated.

Achieving high ionic conductivity relies on the creation of effective paths for long range ion hopping via diffusion channels of reduced activation energy. Structural disordering in the form of vacancies and interstitials sites are also needed and a high polarizability of the anion sub-lattice is desirable for cationic mobility.[10]

Borohydrides are usually kept away from any oxidizing source to avoid any premature liberation of hydrogen and the degradation of their structure.[25] However, a controlled exposure of borohydrides to oxygen could segregate cations on their surface to result in varied defective surface compositions. For example, it has been reported that oxidation of $LiBH_4$ leads to a surface segregation of Li, and thus significant disproportion of the surface composition including the formation of various oxides such as Li_2O and $Li_xB_yO_zH_m$.[26]

In this study, we investigated the possibility of creating defects through the oxidation of borohydrides and in particular $NaBH_4$. By simply exposing $NaBH_4$ to air, we have found that surface oxidation enabled significant improvement in the ionic conductivity of $NaBH_4$ at room temperature. Through a more controlled oxidation, we found that exposure of $NaBH_4$ to 5% of oxygen (O_2) was sufficient to lead to high ionic conductivity. More remarkably, this extremely simple process was also found to enhance the conductivity of $LiBH_4$ and $Mg(BH_4)_2$ to levels several-orders of magnitude higher than that of their pristine forms. The strategy reported here provides, for the first time, new ways to achieve superionic conduction in solid-state electrolytes comprising of complex borohydrides by an extremely simple approach.

2. Result and Discussion

2.1. Effect of Exposure of $NaBH_4$ to Air on Its Ionic Conduction

As per previous reports,[27] $NaBH_4$ has a low ionic conductivity < 10^{-10} S cm^{-1} at room temperature (**Figure 1**a,c). The Nyquist plot for pristine $NaBH_4$ at the ambient consisted of a single semi-circle owing to the bulk/grain boundary (Figure 1a). Upon heating, the ionic conductivity slightly increased to reach 5.13×10^{-8} S cm^{-1} at 105 °C (Figure 1c). Unlike $LiBH_4$, $NaBH_4$ does not undergoes any "favorable" phase transition upon heating.[28] $NaBH_4$ cubic crystalline structure does not allow for obstructed Na^+ diffusion, fast BH_4^- rotational motion, and sufficient interstitial sites for Na^+ jumps.[29]

$NaBH_4$ is known to be stable in air, and unlike some of its parent compounds, for example, $LiBH_4$, partial oxidation of $NaBH_4$ does not lead to a rapid decomposition of the borohydride and elemental segregation into oxides of Na and B.[26] Based on these observations and taking into consideration the hypothesis of fast Li^+ diffusion at the oxidized interface of $LiBH_4$ nanoconfined in porous silica,[22] we hypothesized that direct oxidation of $NaBH_4$, could potentially lead to the creation of vacancies prone to facilitate Na^+ diffusion.

Once exposed to ambient air for 1 h, and transferred back to a high purity Argon atmosphere, the partial oxidation of $NaBH_4$ resulted in a significant increase of the ionic conductivity from 6.90×10^{-11} to 1.63×10^{-5} S cm^{-1} at 20 °C (Figure 1c). In contrast to pristine $NaBH_4$, the Nyquist plot of air oxidized $NaBH_4$ exhibited only one spike (Figure 1b), which was ascribed to the electrode contribution. This behavior is similar to that of sulfide conductors,[30] which typically have low grain boundary resistance. The highest ionic conductivity (2.51×10^{-4} S cm^{-1}) achievable with air oxidized $NaBH_4$ was observed at 35 °C.

At higher temperatures, the conductivity started to decrease to 4.01×10^{-6} S cm^{-1} at 100 °C. But even at such a temperature, the measured ionic conductivity of air oxidized $NaBH_4$ is two orders of magnitude higher than for pristine $NaBH_4$. Unlike previous observations on the ionic conductivity of borohydrides, the trends of ionic conductivity of oxidized $NaBH_4$ are not monotonic with increasing temperatures.[14a] Our initial assumption is that the improvement of ionic conductivity observed is due to the generation of vacancies on the $NaBH_4$ surface owing to a partial oxidation of the surface. Further heating of the oxidized compound may facilitate vacancies annealing and re-crystallization of non-conductive oxide phases.

This finding is remarkable. Not only high ionic conductivity was reached with $NaBH_4$, but this was achieved through an extremely simple approach. To date, the best ionic conductivities reported are those based on the introduction of large size anions such as $[B_{12}H_{12}]^{2-}$, $[B_{10}H_{10}]^{2-}$, and $CB_9H_{10}^-$,[23a] with $NaCB_9H_{10}$ showing the highest conductivity of 0.03 S cm^{-1} at 25 °C.[24] However, the synthesis of $NaCB_9H_{10}$ is not straightforward,[31] and the compound, although commercially available, is as expensive as platinum, strictly controlled owing to the potential of boron rich compounds for military application, and thus unlikely to be produced at large scale at a competitive cost. The mixed borane anionic $Na_3B_{12}H_{12}BH_4$ compound also showed a conductivity of 5×10^{-4} S cm^{-1} at room temperature, but the synthesis of such compounds is more difficult than the

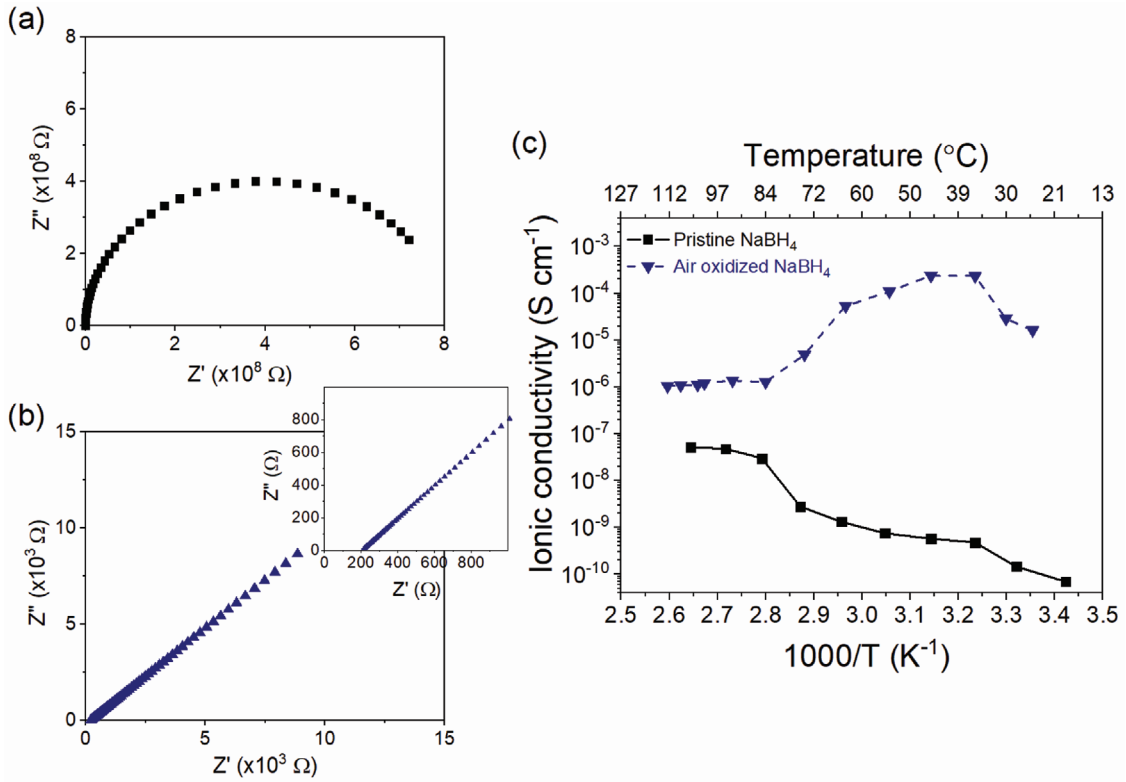

Figure 1. Nyquist plot of a) pristine $NaBH_4$, b) $NaBH_4$ oxidized for 1 h by exposure to ambient air. Measurements were done at 35 °C under an inert Argon atmosphere; and c) Arrhenius plot of the ionic conductivities of pristine and oxidized $NaBH_4$.

simple approach of $NaBH_4$ partial surface oxidation.[32] The next sodium borohydride compounds reported so far are those based $[B_{12}H_{12}]^{2-}$, $[B_{10}H_{10}]^{2-}$ with conductivities < 10^{-7} S cm^{-1} at the ambient.

2.2. Improving the Ionic Conductivity of $NaBH_4$ through Controlled Oxidation

In order to determine the highest possible ionic conductivity reachable through the simple oxidation of $NaBH_4$, controlled experiments were designed where $NaBH_4$ was subjected to fixed concentrations of O_2. The results of such an approach are summarized in **Figure 2**a and Figure S1, Supporting Information, with the highest conductivity of 2.50 mS cm^{-1} reached when $NaBH_4$ was subjected to 5% O_2 in Argon for 1 h. At inferior O_2 concentrations the conductivity was lower, and upon subjecting $NaBH_4$ to higher concentration of O_2, the ionic conductivity decreased. This may be interpreted as an excessive surface oxidation of $NaBH_4$.

XRD analysis of $NaBH_4$ exposed to 5% O_2 did not reveal any boron or sodium oxide phases but only diffraction peaks related to the well-known $NaBH_4$ cubic phase[26] (Figure S2a, Supporting Information). The strong $NaBH_4$ diffraction peaks and the lack of visible oxide phases confirms that the oxidation is limited to the surface of the $NaBH_4$ particles. This also suggests that the oxidized surface layer is amorphous and/or lacks long-range crystallinity.[33] The small shift of diffraction peaks observed for oxidized $NaBH_4$ to the lower Bragg's angles as compared to pristine $NaBH_4$, however suggested a defective crystalline structure (Figure S3, Supporting Information).[34]

Calculating the crystalline size of the materials by using the Scherrer equation revealed a small decrease in the crystal size of oxidized $NaBH_4$ (29 ± 2 nm) as compared to pristine and ball milled $NaBH_4$ (35 ± 2 nm). Such a small decrease in crystallite size may not be sufficient to explain the drastic improvement observed in ionic conductivity upon the oxidation of $NaBH_4$. Indeed, ball-milling alone did not result in an improvement of the ionic conductivity of $NaBH_4$ (Figure S4, Supporting Information). In order to confirm the amount of oxidized $NaBH_4$, the material was subjected to TGA, but given the large evaporation of molten Na in addition to hydrogen, it was difficult to conclude on the level of oxidation of the borohydride (Figure S5, Supporting Information).

Fourier Transformed Infrared (FTIR) analysis confirmed a partial oxidation of $NaBH_4$ exposed to 5% O_2 (**Figure 3**). By FTIR, the typical B—H stretching vibrations corresponding to the BH_4^- anion were observed in the range 2200 to 2400 cm^{-1}.

The B—H bending mode of $NaBH_4$ was also apparent at 1129 cm^{-1} in agreement with previous reports,[35] and this further validated the hypothesis of partial oxidation of $NaBH_4$ once exposed to 5% O_2. Indeed, as compared to pristine $NaBH_4$, the FTIR spectrum of the oxidized material showed additional vibrations corresponding to O—H stretching at around 3500 cm^{-1}, B—O—H bending modes in the range 1500–1250 cm^{-1} as well as B—O stretching modes in the range 950–750 cm^{-1}.[36] No vibrations corresponding to sodium oxide/hydroxides were observed.[37] Furthermore, owing to the lack of the strong characteristic vibrations related to boric acid compounds at 1450 and

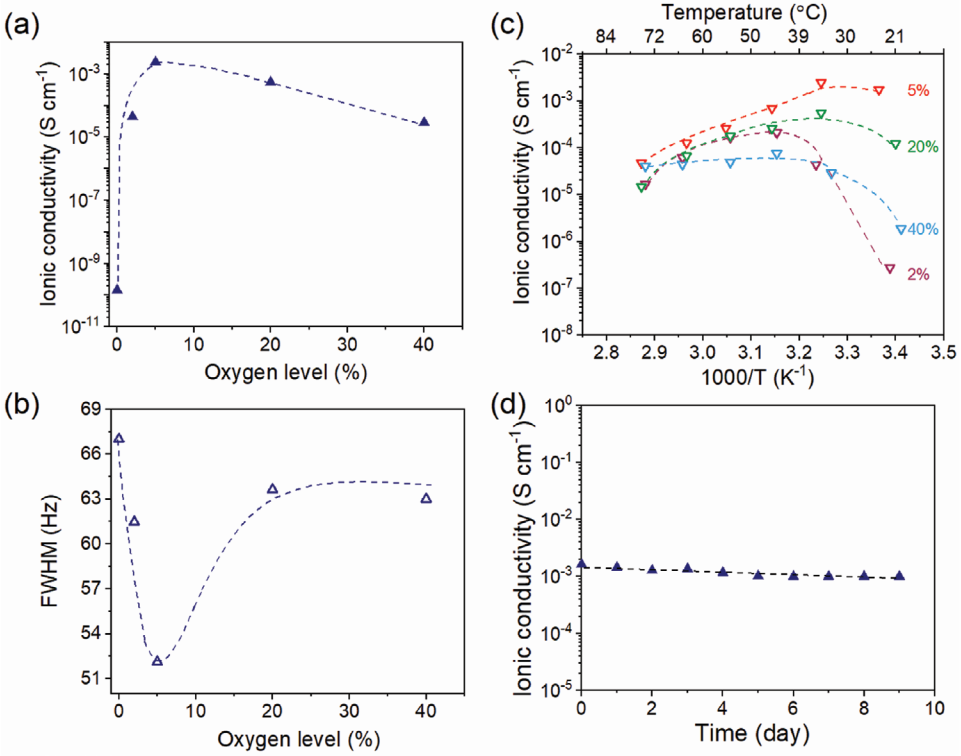

Figure 2. a) $NaBH_4$ ionic conductivity at 35 °C as function of O_2 levels, b) ^{23}Na NMR Full Width at Half Maximum (FWHM) of $NaBH_4$ oxidized by different O_2 levels, c) ionic conductivity of $NaBH_4$ oxidized at different O_2 levels as function of temperature, and d) stability of the ionic conductivity at 35 °C of $NaBH_4$ exposed to 5% O_2.

815 cm^{-1},[38] the observed B—O and B—O—H vibrations were considered to originate from hydrated $NaBO_2$ resulting from the exposure of $NaBH_4$ to 5% O_2.[36] Solid state ^{11}B NMR analysis of oxidized $NaBH_4$ also revealed a single sharp peak at 1.9 ppm, which was assigned to the tetrahedrally co-ordinated B—O (**Figure 4**),[39] and this is consistent with the interpretation of the FTIR results and the formation of $NaBO_2$. Additional XRD of $NaBH_4$ exposed to 5% O_2 and heat treated for several hours also confirmed the crystallization of the $NaBO_2$ trigonal phase (Figure S2b, Supporting Information).

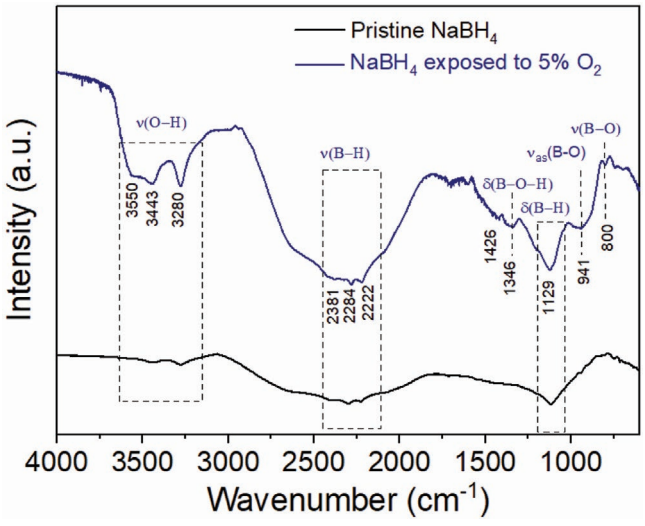

Figure 3. FTIR spectrum of $NaBH_4$ exposed to 5% O_2 as compared to the FTIR spectrum of pristine $NaBH_4$.

The ^{11}B NMR spectrum of oxidized $NaBH_4$ also showed the typical resonance of the BH_4^- anion centered at −42.06 ppm (Figure 4), in agreement with previous studies.[40] Comparison of the ^{11}B MAS spectrum of oxidized $NaBH_4$ with that of pristine $NaBH_4$ (Figure 4), further indicated a significant broadening of the BH_4^- peak and this was interpreted as a reduction of the crystal ordering upon oxidation. As further shown in Figure 2b and Figure S6, Supporting Information, the full width at half maximum (FWHM) of ^{23}Na NMR spectrum was found to also evolve as function of the level of oxidation of $NaBH_4$ in agreement with the evolution of Na ionic conductivity as function of the oxidation level of $NaBH_4$ (Figure 2a,b). Increased ionic mobility should be associated with a narrowing of the NMR peak linewidth, as this reduces or averages away line broadening caused by chemical shift distribution, dipolar coupling, and quadrupolar couplings. In the case of $NaBH_4$, which has a cubic symmetry, the quadrupolar interaction is ≈0 kHz, while application of heteronuclear decoupling removes the dipolar interactions resulting in a single sharp peak at −15 ppm.[41] Thus the primary source of line broadening is the chemical shift dispersion caused by defects/disorder in the material. Pristine $NaBH_4$ has the narrowest ^{23}Na linewidth (FWHM of 50.23 Hz), which is consistent with its highly ordered structure and concomitantly minimal chemical shift dispersion (Figure 2b and Figure S6, Supporting Information). The initial ball milling step of the $NaBH_4$ results in increased bond disorder of the crystalline material, which causes a

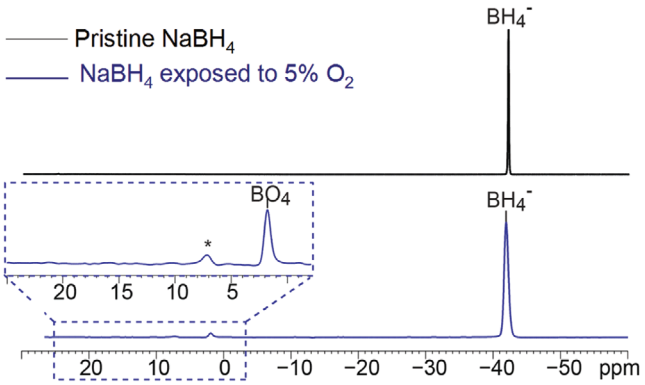

Figure 4. Solid-state ^{11}B NMR of pristine $NaBH_4$ and $NaBH_4$ exposed to 5% O_2. BO_4 represents B tetrahedrally coordinated to O and * represents spinning sidebands.

chemical shift dispersion, and this is observed as an increase in the ^{23}Na NMR linewidth (FWHM of 67.01 Hz, Figure S6, Supporting Information). Upon successive oxidation steps from 2% to 40% of O_2, the ^{23}Na NMR linewidth first decreases with the narrowest linewidth obtained at the 5% O_2 and thereafter increases up to 63 Hz FWHM, with no significant difference between the 20% and 40% O_2. These results closely map the results of the EIS, and indicate that excessive oxidation retards the ionic mobility. At high O_2 levels, the increased coverage of the $NaBH_4$ particle surface by an insulating oxide layer may block ionic diffusion paths. Upon temperature variations, the highest ionic conductivity of $NaBH_4$ exposed to 5% O_2 was reached at 35 °C (2.5×10^{-3} S cm^{-1}) and then decreased to 4.79×10^{-5} S cm^{-1} (Figure 2c).

It should be noted that the ^{1}H NMR of $NaBH_4$ exposed to 5% O_2 confirmed the absences of water and H^+ compounds in the material (Figure S7, Supporting Information), and this further evidenced that the conductivity observed was solely due to Na^+ diffusion.

To further understand and characterize the high ionic conductivity observed in oxidized $NaBH_4$, first-principles simulations based on density functional theory (DFT) were performed. Ionic diffusion involves highly anharmonic and temperature dependent processes; hence we employed ab initio molecular dynamics to simulate these.[33] In particular, the mean-squared (MSD) and diffusion coefficient (D) features of $NaBH_4$ within the temperature interval $25 < T < 475$ °C were estimated. The DFT results as summarized in **Figure 5** show that sodium diffusivity in perfectly stoichiometric $NaBH_4$ is practically null at temperatures as high as 475 °C (the corresponding MSD is manifestly flat at long simulation times, hence $D \approx 0$). Nevertheless, when a small concentration of sodium vacancies (≈2%) is considered in the simulations, the material ionic diffusivity increases significantly (Figure 5b). This result suggests that ionic conductivity in $NaBH_4$, and possibly also in other complex borohydrides, is vacancy mediated. For instance,

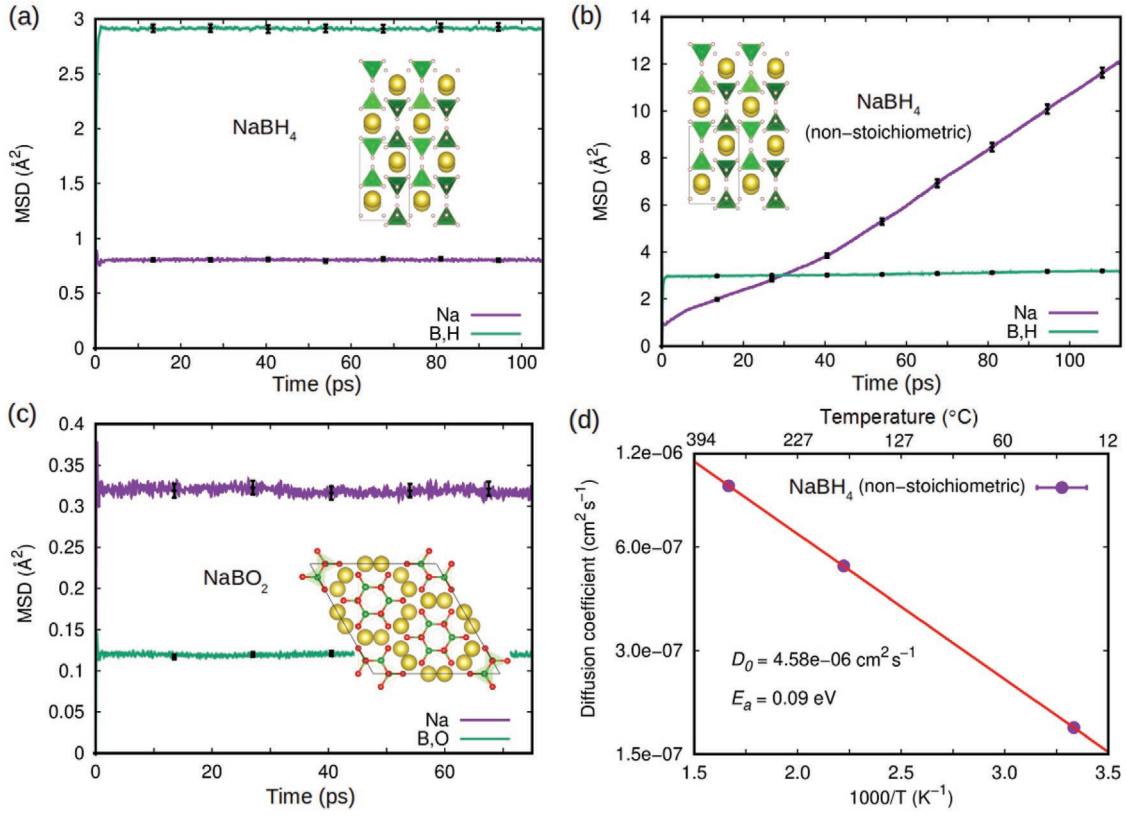

Figure 5. DFT calculations on the ionic transport properties of $NaBH_4$ (cubic Fm-3m) and $NaBO_2$ (rhombohedral R-3c). Mean-squared displacement (MDS) calculated in a) stoichiometric $NaBH_4$, b) off-stoichiometric $NaBH_4$, and c) $NaBO_2$ at $T = 475$ °C. d) Arrhenius plot of the ionic diffusivity estimated in off-stoichiometric $NaBH_4$.

at temperatures close to 25 °C the computed D for off-stoichiometric $NaBH_4$ is of the order of 10^{-7} cm^2 s^{-1} (Figure 5d). This is comparable to the values obtained in archetypal lithium-based conductors at similar conditions.[33] Specifically, we calculated a pre-exponential factor and activation energy for ion migration of $\approx 5 \times 10^{-6}$ cm^2 s^{-1} and 0.1 eV in off-stoichiometric $NaBH_4$. The presence of sodium vacancies in oxidized $NaBH_4$ can be rationalized in terms of cation segregation toward the nanoparticle surface upon oxidation,[26] with possible formation of tetraborate species therein, as confirmed by XRD (Figure S3b, Supporting Information). To confirm the potential role of oxides, the ionic transport properties of amorphous $NaBO_2$ was also analyzed and found to be not conducting ($D \approx 0$, Figure 5c). From these simulation results, it can be suggested that the ionic conductivity in oxidized $NaBH_4$ particles is mostly taking place within the interior of the particles, not in their surfaces, and this is consistent with experimental observations as the $NaBO_2$ phase has been found to crystallize with increasing temperatures, while the ionic conductivity of ionic $NaBH_4$ still remains high (Figure 2).

Further investigation regarding the stability of $NaBH_4$ oxidized systems indicated that their high ionic conductivity ($\approx 10^{-3}$ S cm^{-1}) was retained for several days (Figure 2d), and remained stable upon heating and cooling cycles from 20 to 45 °C (Figure S8, Supporting Information). No degradation was observed, and this suggested that once oxidized $NaBH_4$ is a stable ionic conductor. Additional, CV measurement conducted on an asymmetric cell consisting of Na as one of the electrodes, demonstrated the actual plating and stripping of sodium and thus the actual transport of Na^+ across the pellet of $NaBH_4$ exposed to 5% O_2 (Figure S9, Supporting Information). Furthermore, the Na^+ transference number was determined to be 0.92 (Figure S10, Supporting Information) and this suggest that the current through the electrolyte is ionic.

2.3. Improving the Ionic Conductivity of Other Borohydrides through Oxidation

Other borohydrides of interest as solid state electrolytes are those based on lithium and magnesium. In the $NaBH_4$ system, the highest ionic conductivity was reached upon exposure of the borohydride to 5% O_2. The same level of oxidation was thus tested on $LiBH_4$ and $Mg(BH_4)_2$.

The Nyquist plot of pristine $LiBH_4$ resulting from the impedance measurement consisted of one semi-circle and one spike in the low-frequency region (Figure S11a, Supporting Information), which corresponds to the contribution of the bulk/grain boundary and the electrode, respectively. After exposing $LiBH_4$ to 5% O_2 the Nyquist plot turned to one spike (Figure S11b, Supporting Information), akin oxidized $NaBH_4$. Comparing ionic conductivities (**Figure 6**a), that of oxidized $LiBH_4$ (1.97×10^{-4} S cm^{-1}) at 35 °C is five order of magnitude higher than that of pristine $LiBH_4$. Overall, the ionic conductivity of oxidized $LiBH_4$ reaches 1.88 mS cm^{-1} at 55 °C. This is the highest ionic conductivity reported so-far for $LiBH_4$ based solid-state electrolytes. For comparison the ionic conductivity of $LiBH_4$ nanoconfined in SiO_2[22] or lithium carborane incorporating large cations including $CB_9H_{10}^-$ and $CB_{11}H_{12}^-$ is below or around 0.2 mS cm^{-1} at the same temperature.[14a]

When exposing $Mg(BH_4)_2$ to 5% O_2, the same observations were made and the ionic conductivity reached 7.89×10^{-6} S cm^{-1} at room temperature (Figure 6b and Figure S12, Supporting Information). This is significantly higher than the very low ionic conductivity of pristine $Mg(BH_4)_2$ (9.63×10^{-13} S cm^{-1} at 25 °C—Figure S12, Supporting Information). The ionic conductivity reached upon oxidation of $Mg(BH_4)_2$ is the highest reported so far. To date, the best possible ionic conductivity has been reported upon the modification of $Mg(BH_4)_2$ with ethylenediamine leading to an ionic conductivity of 5×10^{-8} S cm^{-1} at 30 °C.[42] Modification with ammonia enabled an ionic conductivity of 3×10^{-6} S cm^{-1} at 100 °C.[21] The very low conductivity of pristine $Mg(BH_4)_2$ is attributed to its structure in which the Mg^{2+} ions are seating in firm tetrahedral cages composed of four BH_4^- units with strong coulombic interaction.[43]

The actual Li^+ and Mg^{2+} ion transport upon oxidation of their respective borohydride was further confirmed by CV measurements showing peaks related to their relative deposition and stripping (Figures S13 and S14, Supporting Information). Once again, it is believed that the improvements observed are the result of the vacancies generated upon surface oxidation.

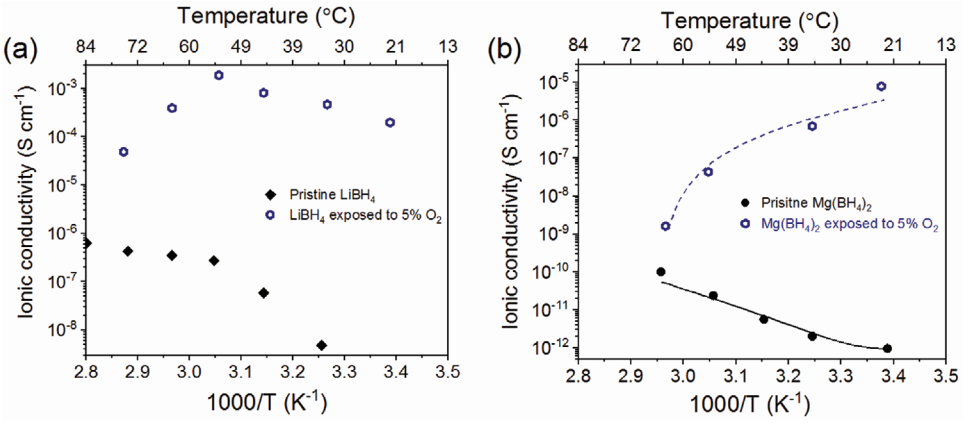

Figure 6. a) Arrhenius plot of a) $LiBH_4$ exposed to 5% O_2 compared with that of pristine $LiBH_4$, and b) $Mg(BH_4)_2$ exposed to 5% O_2 compared with that of pristine $Mg(BH_4)_2$. From the slope of the Arrhenius plot up to 50 °C, the activation energy of pristine $LiBH_4$ was determined to be of 0.7 eV with a pre-exponential factor of 2.4 10^4 s^{-1}, while that of oxidized $LiBH_4$ was found to be of 0.53 eV with a pre-exponential factor of 8.3 10^8 s^{-1}.

However, for all these oxidized borohydrides, it should be noted that once the temperature is increased the conductivity decreases (Figure 6), and this is believed to be the result of the crystallization of the oxide phase and partial annealing of vacancies.

XRD analysis of oxidized $LiBH_4$ and $Mg(BH_4)_2$ did not show any new phases, except those corresponding to the respective borohydrides (Figure S15, Supporting Information). However, FTIR analysis confirmed the formation of oxide phases in both materials (Figures S16 and S17, Supporting Information). From FTIR analysis the exact natures of these oxides is difficult to confirm owing to a possible segregation of Li and Mg on the borohydride particle surface and the formation of multiple oxides.[26] However, the various vibrations recorded for oxidized $LiBH_4$ would tend to confirm the formation of $Li_2B_4O_7$ and LiB_5O_8.[36] In the case of $Mg(BH_4)_2$ the oxide stretching vibrations may be related to $Mg_2B_6O_{11}$ and MgB_6O_{10} compounds.[36] According to the interpretation of the FTIR spectrum, both lithium and magnesium borates contain B sites tri and tetra coordinated to O and this is in agreement with the NMR analysis of the oxidized $LiBH_4$ and $Mg(BH_4)_2$ compounds (Figures S18 and S19, Supporting Information). Once, again our attempts to quantify the amount of the oxides phases by TGA were unsuccessful (Figures S20 and S21, Supporting Information), because of the complex decomposition path of borohydrides. By FTIR and NMR analysis it was also found that a $MgB_{12}H_{12}$ traces appeared in $Mg(BH_4)_2$ upon oxidation (Figures S17 and S19, Supporting Information). This may be due to the release of diborane (B_2H_6) during the partial oxidation of the borohydride, since further reaction of B_2H_6 with $Mg(BH_4)_2$ is known to lead to the formation of $MgB_{12}H_{12}$.[44] The role of $MgB_{12}H_{12}$ in facilitating the improvement in ionic conductivity observed for oxidized $Mg(BH_4)_2$ should be considered. However, the ionic conductivity of $MgB_{12}H_{12}$ has been predicted to be poor.[36,45]

3. Conclusions

We report on the effect of oxidation to significantly enhance the ionic conductivity of complex borohydrides including $NaBH_4$, $LiBH_4$, and $Mg(BH_4)_2$. Simple exposure of $NaBH_4$ to ambient air was found to drastically improve Na^+ conduction from 6.90×10^{-11} to 1.63×10^{-5} S cm^{-1} at 20 °C. Upon a controlled oxidation of $NaBH_4$ with 5% O_2 in Argon, this conductivity reached 2.5×10^{-3} S cm^{-1} at 35 °C. Such a very high ionic conductivity was found to be stable for several days and effectively lead to sodium stripping and plating. Similar observations were made for $LiBH_4$ and $Mg(BH_4)_2$ with a significant improvement of their ionic conductivity upon oxidation, and this demonstrates the potential of the approach in leading to super-ionic conductors based on borohydrides. Such an improvement is believed to be the result of the formation of vacancies within the borohydride particles upon cation segregation during surface oxidation. Ionic conduction would occur within the borohydride particles as opposed to the hypothesis of higher diffusion at oxidized surfaces. A better understanding of the vacancies generated upon the surface oxidation of borohydrides and the ionic diffusion mechanism is expected to allow further increase in ionic conductivity. Our approach that is extremely simple to implement, point toward a novel strategy to design low-temperature solid state ionic conductors for all solid state batteries utilizing abundant elements such as sodium and magnesium.

4. Experimental Section

All operations and material handling were carried out under inert atmosphere in an Argon-filled LC-Technology glove box (<1 ppm O_2 and H_2O). Sodium borohydride ($NaBH_4$, 99%) was purchased from Sigma-Aldrich. Lithium borohydride ($LiBH_4$, 95%) was purchased from Acros. Prior use, $LiBH_4$ was purified following the reported procedures.[46] Magnesium borohydride ($Mg(BH_4)_2$) was synthesized as per previous reports.[47]

Complex Borohydrides Oxidation: Before exposure to O_2, all the borohydrides (120 mg) were ball-milled under high purity Argon in a 15 ml stainless steel vial filled with a single stainless steel ball (1.5 g and 15 mm diameter). The ball milling was carried out with a Retsch MM301 mill operated at a frequency of 20 Hz for 10 min.

After ball milling the borohydride powder was transferred under Argon in a home-made sample holder. The later was then evacuated to 0.1 kPa to remove the Argon and a known amount of O_2 in Argon was injected in the sample holder until a pressure of 0.1 MPa was reached. $NaBH_4$ was left to oxidize for 1 h, while $LiBH_4$ and $Mg(BH_4)_2$ were reacted with O_2 for 10 min. The oxidized powder was finally cold-pressed by using a 10 mm die and a hydraulic press maintained at 9 MPa for 30 min. The borohydride pellet (0.3 mm thickness and 71.2 mm^2) was placed under Argon in a controlled environment sample holder (CESH) from BioLogic for impedance measurement.

Characterization: The crystalline nature of the materials was determined by X-ray Diffraction (XRD) using a Philips X'pert Multipurpose XRD system operated at 40 mA and 45 kV with a monochromated Cu Kα radiation (λ = 1.541 Å)—step size = 0.01° and time per step = 20 s. During XRD measurement, the materials were protected against oxidation from the air by a Kapton foil.

Phase transitions and hydrogen release profiles were determined by Thermogravimetric Analysis (TGA) and Differential Scanning Calorimetry (DSC) in conjunction with Mass Spectrometry (MS) by using a Mettler Toledo TGA/DSC 1 coupled with a Pfeiffer OmniStar MS. 70 µL alumina crucibles were used and analyses were conducted at a heating rate of 10 °C min^{-1} under an Argon flow of 20 mL min^{-1}.

FTIR characterizations were carried out on a Bruker Vertex 70 V equipped with a Harrick Diffuse Reflectance Infrared Fourier Transform Spectroscopy (DRIFTS) Praying Mantis accessory. The materials were loaded in an air-tight chamber in the glovebox and the chamber was fitted on the Praying Mantis. Spectra were acquired with a 1 cm^{-1} resolution with an MCT-detector.

Solid-state ^{11}B, and ^{23}Na Magic Angle Spinning (MAS) Nuclear Magnetic Resonance (NMR) experiments were carried out on a narrow-bore Bruker Biospin Avance III solids–700 MHz spectrometer with a 16.4 Tesla superconducting magnet operating at frequencies of 700 MHz, 224.7 MHz, and 185 MHz for the ^{1}H, ^{11}B, and ^{23}Na nuclei respectively. Approximately 3–10 mg of material was packed into 4 or 2.5 mm zirconia rotors fitted with Kel-f caps or vespel caps, respectively. The 4 mm rotors were spun in a double resonance H-X probe head at 14 kHz at the magic angle, while the 2.5 mm rotors were spun to 20 kHz at the magic angle. The ^{11}B and ^{23}Na spectra were acquired with a hard 1 to 3 µs radio frequency pulses corresponding to a 30° tip angle. The recycle delays of up to 10 s were used to ensure full relaxation of the signals of all nuclei, and up to 512 transients were co-added to ensure sufficient signal to noise. The ^{11}B NMR shifts were referenced to liquid $F_3BO.O(C_2H_5)_2$ at 0 ppm using solid $NaBH_4$ at –42.06 ppm as a secondary reference. ^{23}Na NMR shifts were referenced to 1 M NaCl(aq) at 0 ppm. SPINAL decoupling at a field strength of 90 kHz was used to decouple the ^{1}H nuclei. The spectral deconvolution was carried out using the Dmfit software.[48]

Electrochemical Impedance Spectroscopy (EIS) were conducted by using the AC impedance spectroscopy method with a VMP3 potentiostat (BioLogic). Frequencies from 100 mHz to 1 MHz were used. The measurements were conducted between 25 and 120 °C. Before each measurement the sample was dwelled for 30 min for temperature equilibration. The Nyquist plots were fitted using an equivalent model circuit and the ionic conductivity σ was calculated from

$$\sigma = d/AR \tag{1}$$

where d is the thickness of the pressed borohydride, A is the surface area of the pellet and R is the pellet resistance determined from the intersection of the semicircle with the Z' axis at high frequency.

Cyclic Voltammetry measurement (CV) of oxidized $NaBH_4$ was performed on an asymmetric cell made of a stainless steel foil/$NaBH_4$ exposed to 5% O_2/Na/stainless steel and the potential was decreased from 1.2 to –1 V at a scan rate of 1 mV s^{-1}. Cationic transport numbers (t^+) of oxidized $NaBH_4$ was measured and calculated by Alternating Current (AC) impedance and Direct Current (DC) polarization with a DC voltage of 10 mV with two non-blocking electrodes in the configuration Na/ $NaBH_4$ exposed to 5% O_2/Na using a typical Swagelok cell.

Density Functional Theory Calculations: To help the understanding of the experimental observations, first-principles calculations based on Density Functional Theory (DFT) were performed to analyze the ionic transport properties of $NaBH_4$ and sodium metaborate ($NaBO_2$), as representative systems. The calculations were done with the VASP code[49] using the generalized gradient approximation to the exchange-correlation energy due to Perdew et al.[50] (possible dispersion interactions in the crystals were captured with the *D3* correction scheme developed by Grimme et al.).[51] The projector-augmented-wave method was employed to represent the ionic cores and the following electronic states were considered as valence: Na 2p-3s, B 2s-2p, O 2s-2p, and H 1s. Wave functions were represented in a plane-wave basis truncated at 650 eV. In the geometry relaxations, a tolerance of 0.01 eVÅ^{-1} was imposed on the atomic forces. By using these parameters and dense k-point grids for Brillouin zone integration, the energies of the optimized systems converged within 1 meV per formula unit.

Ab Initio Molecular Dynamics (AIMD) simulations based on DFT were performed in the canonical (*N,V,T*) ensemble (constant number of particles, volume, and temperature). The temperature in the AIMD simulations was kept fluctuating around a set-point value by using Nose–Hoover thermostats. Large simulation boxes containing 288 and 312 atoms (for $NaBH_4$ and $NaBO_2$, respectively) were employed and periodic boundary conditions were applied along the three Cartesian directions. Non-stoichiometric systems were generated by removing just one sodium atom from the simulation cell. Newton's equations of motion were integrated by using the Verlet algorithm and a timestep of 10^{-3} ps. Γ-point sampling for Brillouin zone integration was employed in all AIMD simulations. The calculations comprise long simulation times of ≈200 ps and for each compound a total of 8 AIMD simulations at different temperatures considering stoichiometric and off-stoichiometric compositions.

To analyze the ionic transport properties of the selected compounds, their mean-squared displacement (MSD), $\Delta r^2(t)$, and diffusion coefficient, D is computed. The mean-squared displacement of each ionic species was defined as:

$$\left\langle \Delta r_i^2(t) \right\rangle = \left\langle \left| r_i(t+t_o) - r_i(t_0) \right|^2 \right\rangle \tag{2}$$

where $r_i(t)$ is the position of the migrating ion labeled as i at time t, t_0 is an arbitrary time origin, and ⟨...⟩ denotes the average over time origins and ions (averaging over t_0 allowed us to accumulate enough statistics to reduce significantly the MSD fluctuations at long times.[52]

The diffusion coefficient was defined as:

$$D = \lim_{t\to\infty} \frac{\left\langle \left| r_i(t+t_o) - r_i(t_o) \right|^2 \right\rangle}{6t} \tag{3}$$

In our simulations, the T dependence of the diffusion coefficient is assumed to follow the Arrhenius formula:

$$D(T) = D_0 e^{-\frac{E_a}{k_B T}} \tag{4}$$

where D_0 is a pre-exponential factor, E_a the activation energy for ionic migration, and k_B the Boltzmann constant.

Supporting Information

Supporting Information is available from the Wiley Online Library or from the author.

Acknowledgements

Financial support by UNSW Internal Research Grant program is gratefully acknowledged along with the Office of Naval Research (Award No: ONRG-NICOP-N62909-16-1-2155). The authors appreciate the use of instruments in the Mark Wainwright Analytical Centre at UNSW as well as equipment funded by the Australian Research Council (ARC) Linkage, Infrastructure, Equipment, and Facilities (LIEF). C.C. acknowledges financial support from the Australian Research Council's Future Fellowship funding scheme (No. FT140100135). Computational resources and technical assistance were provided by the Australian Government and the Government of Western Australia through Magnus under the National Computational Merit Allocation Scheme and The Pawsey Supercomputing Centre.

Conflict of Interest

The authors declare no conflict of interest.

Keywords

batteries, complex borohydrides, ionic conductors, oxidation

Received: October 22, 2019
Revised: January 11, 2020
Published online:

[1] S. Chen, K. Wen, J. Fan, Y. Bando, D. Golberg, *J. Mater. Chem. A* **2018**, *6*, 11631.
[2] X. K. Wu, K. F. Song, X. Y. Zhang, N. F. Hu, L. Y. Li, W. J. Li, L. Zhang, H. F. Zhang, *Front. Energy Res.* **2019**, *7*, 17.
[3] a) J. B. Goodenough, Y. Kim, *Chem. Mater.* **2010**, *22*, 587; b) B. Scrosati, J. Garche, *J. Power Sources* **2010**, *195*, 2419; c) V. Etacheri, R. Marom, R. Elazari, G. Salitra, D. Aurbach, *Energy Environ. Sci.* **2011**, *4*, 3243.
[4] a) C. Zhao, L. Liu, X. Qi, Y. Lu, F. Wu, J. Zhao, Y. Yu, Y.-S. Hu, L. Chen, *Adv. Energy Mater.* **2018**, *8*, 1703012; b) Z. J. Wu, Z. K. Xie, A. Yoshida, Z. D. Wang, X. G. Hao, A. Abudula, G. Q. Guan, *Renewable Sustainable Energy Rev.* **2019**, *109*, 367; c) P. Verma, P. Maire, P. Novak, *Electrochim. Acta* **2010**, *55*, 6332; d) E. Quartarone, P. Mustarelli, *Chem. Soc. Rev.* **2011**, *40*, 2525.
[5] a) B. L. Ellis, L. F. Nazar, *Curr. Opin. Solid State Mater. Sci.* **2012**, *16*, 168; b) J. Y. Hwang, S. T. Myung, Y. K. Sun, *Chem. Soc. Rev.* **2017**, *46*, 3529.
[6] Y. Sun, P. Guan, Y. Liu, H. Xu, S. Li, D. Chu, *Crit. Rev. Solid State Mater. Sci.* **2019**, *44*, 265.

[7] C. Dietrich, D. A. Weber, S. J. Sedlmaier, S. Indris, S. P. Culver, D. Walter, J. Janek, W. G. Zeier, *J. Mater. Chem. A* **2017**, *5*, 18111.
[8] R. Murugan, V. Thangadurai, W. Weppner, *Angew. Chem., Int. Ed.* **2007**, *46*, 7778.
[9] N. Kamaya, K. Homma, Y. Yamakawa, M. Hirayama, R. Kanno, M. Yonemura, T. Kamiyama, Y. Kato, S. Hama, K. Kawamoto, A. Mitsui, *Nat. Mater.* **2011**, *10*, 682.
[10] Z. Zhang, Y. Shao, B. Lotsch, Y.-S. Hu, H. Li, J. Janek, L. F. Nazar, C.-W. Nan, J. Maier, M. Armand, L. Chen, *Energy Environ. Sci.* **2018**, *11*, 1945.
[11] K. B. Hueso, M. Armand, T. Rojo, *Energy Environ. Sci.* **2013**, *6*, 734.
[12] Q. Ma, M. Guin, S. Naqash, C.-L. Tsai, F. Tietz, O. Guillon, *Chem. Mater.* **2016**, *28*, 4821.
[13] a) U. Warhus, J. Maier, A. Rabenau, *J. Solid State Chem.* **1988**, *72*, 113; b) K. D. Kreuer, U. Warhus, *Mater. Res. Bull.* **1986**, *21*, 357; c) M. Guin, F. Tietz, O. Guillon, *Solid State Ionics* **2016**, *293*, 18.
[14] a) R. Mohtadi, S.-I. Orimo, *Nat. Rev. Mater.* **2017**, *2*, 16091; b) M. Matsuo, Y. Nakamori, S.-I. Orimo, H. Maekawa, H. Takamura, *Appl. Phys. Lett.* **2007**, *91*, 224103.
[15] A. Unemoto, M. Matsuo, S.-I. Orimo, *Adv. Funct. Mater.* **2014**, *24*, 2267.
[16] E. M. Fedneva, V. L. Alpatova, V. I. Mikheeva, *Russ. J. Inorg. Chem.* **1964**, *9*, 826.
[17] a) Y. S. Choi, Y.-S. Lee, D.-J. Choi, K. H. Chae, K. H. Oh, Y. W. Cho, *J. Phys. Chem. C* **2017**, *121*, 26209; b) D. Sveinbjörnsson, J. S. G. Myrdal, D. Blanchard, J. J. Bentzen, T. Hirata, M. B. Mogensen, P. Norby, S.-I. Orimo, T. Vegge, *J. Phys. Chem. C* **2013**, *117*, 3249.
[18] J. S. G. Myrdal, D. Blanchard, D. Sveinbjörnsson, T. Vegge, *J. Phys. Chem. C* **2013**, *117*, 9084.
[19] M. Matsuo, A. Remhof, P. Martelli, R. Caputo, M. Ernst, Y. Miura, T. Sato, H. Oguchi, H. Maekawa, H. Takamura, A. Borgschulte, A. Züttel, S.-I. Orimo, *J. Am. Chem. Soc.* **2009**, *131*, 16389.
[20] M. Matsuo, S. Kuromoto, T. Sato, H. Oguchi, H. Takamura, S.-I. Orimo, *Appl. Phys. Lett.* **2012**, *100*, 203904.
[21] R. Le Ruyet, R. Berthelot, E. Salager, P. Florian, B. Fleutot, R. Janot, *J. Phys. Chem. C* **2019**, *123*, 10756.
[22] D. Blanchard, A. Nale, D. Sveinbjörnsson, T. M. Eggenhuisen, M. H. W. Verkuijlen, Suwarno, T. Vegge, A. P. M. Kentgens, P. E. de Jongh, *Adv. Funct. Mater.* **2015**, *25*, 184.
[23] a) P. E. de Jongh, D. Blanchard, M. Matsuo, T. J. Udovic, S.-I. Orimo, *Appl. Phys. A* **2016**, *122*, 251; b) S. Kim, H. Oguchi, N. Toyama, T. Sato, S. Takagi, T. Otomo, D. Arunkumar, N. Kuwata, J. Kawamura, S.-i. Orimo, *Nat. Commun.* **2019**, *10*, 1081.
[24] W. S. Tang, M. Matsuo, H. Wu, V. Stavila, W. Zhou, A. A. Talin, A. V. Soloninin, R. V. Skoryunov, O. A. Babanova, A. V. Skripov, A. Unemoto, S.-I. Orimo, T. J. Udovic, *Adv. Energy Mater.* **2016**, *6*, 1502237.
[25] Q. Lai, Y. Sun, T. Wang, P. Modi, C. Cazorla, U. B. Demirci, J. R. A. Fernandez, F. Leardini, K.-F. Aguey-Zinsou, *Adv. Sustainable Systems* **2019**, *3*, 1900043.
[26] S. Kato, M. Bielmann, A. Borgschulte, V. Zakaznova-Herzog, A. Remhof, S.-I. Orimo, A. Züttel, *Phys. Chem. Chem. Phys.* **2010**, *12*, 10950.
[27] M. Matsuo, H. Oguchi, T. Sato, H. Takamura, E. Tsuchida, T. Ikeshoji, S.-I. Orimo, *J. Alloys Compd.* **2013**, *580*, S98.
[28] O. A. Babanova, A. V. Soloninin, A. P. Stepanov, A. V. Skripov, Y. Filinchuk, *J. Phys. Chem. C* **2010**, *114*, 3712.
[29] Z. Lu, F. Ciucci, *Chem. Mater.* **2017**, *29*, 9308.
[30] Y. Sun, K. Suzuki, S. Hori, M. Hirayama, R. Kanno, *Chem. Mater.* **2017**, *29*, 5858.
[31] F. Teixidor, C. Vinas, *Science of Synthesis: Houben-Weyl Methods of Molecular Transformations*, Georg Thieme Verlag, Germany **2005**.
[32] Y. Sadikin, M. Brighi, P. Schouwink, R. Černý, *Adv. Energy Mater.* **2015**, *5*, 1501016.
[33] a) M. Wang, L. Ouyang, M. Zeng, J. Liu, C. Peng, H. Shao, M. Zhu, *Int. J. Hydrogen Energy* **2019**, *44*, 7392; b) X. B. Yu, D. M. Grant, G. S. Walker, *J. Phys. Chem. C* **2009**, *113*, 17945.
[34] a) M. A. Krivoglaz, *X-ray and Neutron Diffraction in Nonideal Crystals*, Springer, Berlin, Heidelberg **1996**; b) J. Makinson, J. Lee, S. Magner, R. De Angelis, W. Weins, A. Hieronymus, *Adv. X-Ray Anal.* **2000**, *42*, 407.
[35] R. Gosalawit-Utke, K. Suarez, J. M. Bellosta von Colbe, U. Bösenberg, T. R. Jensen, Y. Cerenius, C. Bonatto Minella, C. Pistidda, G. Barkhordarian, M. Schulze, T. Klassen, R. Bormann, M. Dornheim, *J. Phys. Chem. C* **2011**, *115*, 3762.
[36] L. Jun, X. Shuping, G. Shiyang, *Spectrochim. Acta, Part A* **1995**, *51*, 519.
[37] M. P. Krobok, P. G. Johannsen, W. B. Holzapfel, *J. Phys.: Condens. Matter* **1992**, *4*, 8141.
[38] a) E. F. Medvedev, A. S. Komarevskaya, *Glass Ceram.* **2007**, *64*, 42; b) D. Peak, G. W. Luther, D. L. Sparks, *Geochim. Cosmochim. Acta* **2003**, *67*, 2551.
[39] a) J. F. Stebbins, P. Zhao, S. Kroeker, *Solid State Nucl. Magn. Reson.* **2000**, *16*, 9; b) M. R. Hansen, T. Vosegaard, H. J. Jakobsen, J. Skibsted, *J. Phys. Chem. A* **2004**, *108*, 586.
[40] Z. Łodziana, P. Błoński, Y. Yan, D. Rentsch, A. Remhof, *J. Phys. Chem. C* **2014**, *118*, 6594.
[41] S. R. H. Jensen, L. H. Jepsen, J. Skibsted, T. R. Jensen, *J. Phys. Chem. C* **2015**, *119*, 27919.
[42] E. Roedern, R.-S. Kühnel, A. Remhof, C. Battaglia, *Sci. Rep.* **2017**, *7*, 46189.
[43] T. Ikeshoji, E. Tsuchida, S. Takagi, M. Matsuo, S.-I. Orimo, *RSC Adv.* **2014**, *4*, 1366.
[44] A. Remhof, Y. Yan, D. Rentsch, A. Borgschulte, C. M. Jensen, A. Züttel, *J. Mater. Chem. A* **2014**, *2*, 7244.
[45] J. Cuan, Y. Zhou, T. Zhou, S. Ling, K. Rui, Z. Guo, H. Liu, X. Yu, *Adv. Mater.* **2019**, *31*, 1803533.
[46] L. Banfi, E. Narisano, in *Encyclopedia of Reagents for Organic Synthesis*, John Wiley and Sons, Ltd, Hoboken, New Jersey **2005**.
[47] Q. Lai, K.-F. Aguey-Zinsou, *Sustainable Energy Fuels* **2017**, *1*, 1308.
[48] D. Massiot, F. Fayon, M. Capron, I. King, S. Le Calvé, B. Alonso, J.-O. Durand, B. Bujoli, Z. Gan, G. Hoatson, *Magn. Reson. Chem.* **2002**, *40*, 70.
[49] G. Kresse, J. Furthmüller, *Phys. Rev. B* **1996**, *54*, 11169.
[50] J. P. Perdew, K. Burke, M. Ernzerhof, *Phys. Rev. Lett.* **1996**, *77*, 3865.
[51] S. Grimme, J. Antony, S. Ehrlich, H. Krieg, *J. Chem. Phys.* **2010**, *132*, 154104.
[52] A. K. Sagotra, D. Chu, C. Cazorla, *Phys. Rev. Mater.* **2019**, *3*, 035405.

